Origin of the large recoverable electrostrain in relaxor ferroelectrics

Xiaoqin Ke [1,*] Zhengkai Hong,[1] Yin Zhang,[1] Sen Yang,[1,†] and Yunzhi Wang[2,‡]

[1]*School of Physics, MOE Key Laboratory for Nonequilibrium Synthesis and Modulation of Condensed Matter,*
State Key Laboratory for Mechanical Behavior of Materials, Xi'an Jiaotong University, Xi'an 710049, China
[2]*Department of Materials Science and Engineering, The Ohio State University, Columbus, Ohio 43210, USA*

We investigate the mechanisms responsible for the distinct characteristics of certain relaxor ferroelectrics, which display pinched polarization hysteresis loops and recoverable electrostrains, in contrast to the rectangular-like polarization hysteresis loops and irrecoverable butterfly-shaped electrostrains observed in typical ferroelectrics. Despite the large number of experimental reports on these materials, the origin of their recoverable electrostrains has remained elusive until now. Using a phase-field model, we study a doped ferroelectric system, considering both local electric fields and local phase-transition temperature variations induced by the local compositional heterogeneity. The directions of local electric fields are randomly distributed along one of the four directions of the spontaneous polarizations in the system. The resulting phase diagram reveals the existence of both normal ferroelectrics and relaxor ferroelectrics, with pinched polarization hysteresis loops and recoverable electrostrains appearing only in the latter. Our simulations shed light on the crucial role of strong local electric fields along spontaneous polarization directions caused by point defects in facilitating nucleation of domains with polarization along the same direction. This, in turn, explains the recoverability of the polarization and electrostrain in certain relaxors, as these local fields can help restore the initial domain-structure, polarization, and strain. These findings provide new insights into the origin of recoverable electrostrains in relaxors, which could have implications for the design of relaxors with large recoverable electrostrains.

I. INTRODUCTION

The naturally occurring multidomain state of polarization in ferroelectric materials could transform to a single-domain state upon applying a large external electric field, generating a large electrostrain because of the strong coupling between polarization and strain in ferroelectrics [1]. Upon removing the electric field, however, the metastable single-domain state would not spontaneously return to the initial multidomain state [2] because of barriers associated with domain nucleation and domain wall motion (i.e., domain switching). This make the electrostrain of normal ferroelectrics irrecoverable, characterized by a typical butterfly-shaped electrostrain curve, which greatly limits the practical application of ferroelectrics on devices such as actuators.

Only in some uncommon cases could large recoverable electrostrain occur, such as in aged acceptor-doped ferroelectrics [3], ferroelectrics (with a first-order ferroelectric phase transition) above T_C [4,5], antiferroelectrics [6], and some relaxor ferroelectrics [7–11]. But the recoverability of the electrostrain is not stable upon de-aging (e.g., by heating or field cycling) in aged acceptor-doped ferroelectrics. It is only maintained in a limited temperature range in ferroelectrics above T_C, and it relies on a high actuation field

in antiferroelectrics. On the other hand, the large recoverable electrostrains appearing in relaxor ferroelectrics do not require pre-aging or a large actuation field, and they could be maintained in a relatively broad temperature range. These features make relaxor ferroelectrics promising materials for actuators. Nevertheless, the origin of the large recoverable electrostrain in relaxor ferroelectrics remains unclear despite the large number of experimental studies reported in the literature. Initially it was proposed that the recoverability of polarization and electrostrain appearing in relaxors is due to the antiferroelectric-ferroelectric transitions, but such conjecture was later discarded because there is no evidence of antiferroelectric phases in these systems [7,10]. It is now generally believed that the presence of a nonpolar phase at zero field is responsible for the appearance of the large recoverable electrostrain in relaxors [12]. However, such a theory cannot explain why recoverable electrostrains only appear in some relaxor systems such as $Bi_{0.5}Na_{0.5}TiO_3$-$BaTiO_3$-$K_{0.5}Na_{0.5}NbO_3$ relaxors [7] and La-doped $Pb(Zr_{0.65}Ti_{0.35})O_3$ relaxors [11], but not in others like $BaZr_xTi_{1-x}O_3$ relaxors [13] and La-doped $Pb(Zr_{0.4}Ti_{0.6})O_3$ relaxors [14].

Relaxor ferroelectrics are normally induced by doping a sufficiently large amount of point defects into normal ferroelectrics [15–17]. The random distribution of point defects would lead to local compositional heterogeneity, which could result in two effects, i.e., variation of local phase transition temperature (LPTT effect) and variation of local electric fields (LEF effect) [18–20]. The LPTT effect occurs because the phase transition temperature is a sensitive function of

*kexiaoqin@mail.xjtu.edu.cn
†yangsen@mail.xjtu.edu.cn
‡wang.363@osu.edu

composition, and the LEF effect arises because of the local electric field caused by the size/charge difference between the dopants and host ions. It has been found by computer simulations that both LPTT and LEF effects are responsible for many of the unique characteristics experimentally found in relaxors, such as the formation of nanodomains, the appearance of three characteristic temperatures (T_B, T^*, and T_f), and the frequency dispersion of dielectric permittivity [16,21–23]. However, these simulations have failed to predict the pinched hysteresis loop and the corresponding recoverable electrostrain of relaxors under no mechanical loading reported in the experiments. Thus, it is still unclear why recoverable electrostrains could appear in some relaxors and whether they are also related to these two effects.

In this work, we study systematically the hysteresis loops and electrostrains of a doped ferroelectric system by using phase-field simulations that consider both the LPTT and LEF effects associated with point defects. Different from previous models where the local electric fields are randomly distributed in all directions [16,21,23], our model assumes a random distribution of the local electric fields *only in the directions of spontaneous polarizations* in the ferroelectric system. This is because in real ferroelectric systems, the local electric fields resulting from the point defects do not align in all directions but only along certain specific directions (e.g., the spontaneous polarization directions in many systems) [3,24–26]. The simulation results show that in such a system the normal ferroelectrics exhibit single hysteresis loops and butterfly-shaped electrostrains while the relaxor ferroelectrics display pinched hysteresis loops and recoverable electrostrains, which are consistent with the experimental observations in some relaxor systems [7–11]. The recoverability of the polarization and electrostrain in relaxor ferroelectrics can be attributed primarily to the large local electric fields along one of the spontaneous polarization directions caused by the point defects. These local electric fields could assist in nucleation of domains with polarization along the same direction, and thus the initial multidomain state could recover when the applied external electric field is removed, which results in the pinched polarization hysteresis loop and recoverable electrostrain. When the local electric field directions are not along the spontaneous polarization directions, recoverable electrostrain may not occur because nucleation of new domains would be more difficult, which helps explain why recoverable electrostrains appear in only some relaxor systems but not all of them. This work sheds light on the origin of a pinched hysteresis loop and large recoverable electrostrain in relaxor ferroelectrics, and it may guide the design of relaxor materials with large recoverable electrostrains through defect engineering.

II. PHASE-FIELD MODEL

We consider a perovskite-structured model ferroelectric system doped with nonferroelectric heterovalent defects which would not induce oxygen vacancies (e.g., donor defects). The undoped model ferroelectric undergoes paraelectric cubic (C, $Pm\bar{3}m$) to ferroelectric tetragonal (T, $P4mm$) transition at its Curie temperature, and, as can be seen below, most of its parameters either adopt or are modified from those

of BaTiO$_3$. The point defects are assumed to be randomly distributed in the system and thus local compositional heterogeneity naturally occurs. Although there are a few reports on relaxors with multiple phases [10,17,27], for conventional relaxors such as those in Pb$_{1-x}$La$_x$(Zr$_{0.4}$Ti$_{0.6}$)$_{1-x/4}$O$_3$ and BaZr$_x$Ti$_{1-x}$O$_3$ systems, only one stable phase exists and the point defects would not alter the local symmetry [28,29]. Thus, it is safe to assume in the current study that the point defects would not alter the stable phase (i.e., the tetragonal phase) of the ferroelectric system and the local crystal symmetry. Therefore, the relaxors considered in the current study are away from the interferroelectric phase boundary and have relatively large polarization anisotropy. Similar to our previous work [21], the effects of point defects doping are only characterized by the local phase transition temperature effect and the local electric field effect detailed below.

The nonferroelectric nature of point defects would lead to decreases in Curie temperature with increasing local defect concentration [30–32] (see the composition dependency of the Landau coefficient α below). The heterovalent nature of the point defects would lead to internal electric fields associated with the defect dipoles generated by point defects [33]. Assuming that the defect dipoles can only generate electric fields locally, which is not a bad assumption since the electric field generated by electric dipoles scales inversely with the square of distance, then the magnitude of local electric fields caused by defect dipoles can be assumed to increase with increasing local concertation c. For simplicity, the magnitude of the local electric field is approximated by λc, where λ is set to be 200 kV/cm [22], i.e., $|E_{local}| = \lambda c$. On the other hand, since the point defects are randomly distributed on preferred sites of the crystal lattice [3], the directions of local electric fields should also be randomly distributed. Different from previous models where the directions of local electric fields are assumed to be random along *all directions* [16,21,22], here the directions of local electric fields are assumed to be random along *only the four spontaneous polarization directions*: [01], [10], [0$\bar{1}$], and [$\bar{1}$0]. Such an assumption is based on the fact that in doped ferroelectric systems, the local electric fields induced by the point defects are usually aligned only along some specific directions rather than along all directions, and in many cases they are along the spontaneous polarization directions [3,24–26]. Since the relaxors modeled in this work contain a negligible amount of oxygen vacancies, the defects are considered to be static with temperature changing in the studied temperature range as well as under external electric fields. Thus it is assumed that the magnitude and directions of local electric fields do not change with temperature and external electric fields in the studied temperature range and external electric field range. Note that the nonferroelectric heterovalent defects might also cause local strain fields, which could also influence the property of the doped ferroelectric systems [22,33]. However, in the current model, the effect of the local strain fields on the shape of electrostrain is neglected in order to focus on the effect of local electric fields, which is believed to play a significant role in the formation and properties of relaxors [33].

Figure 1(a) plots the distribution of local defect concentration (c) for samples with different $\bar{c}$ as well as the volume fraction of grid points with different c. Note that here the
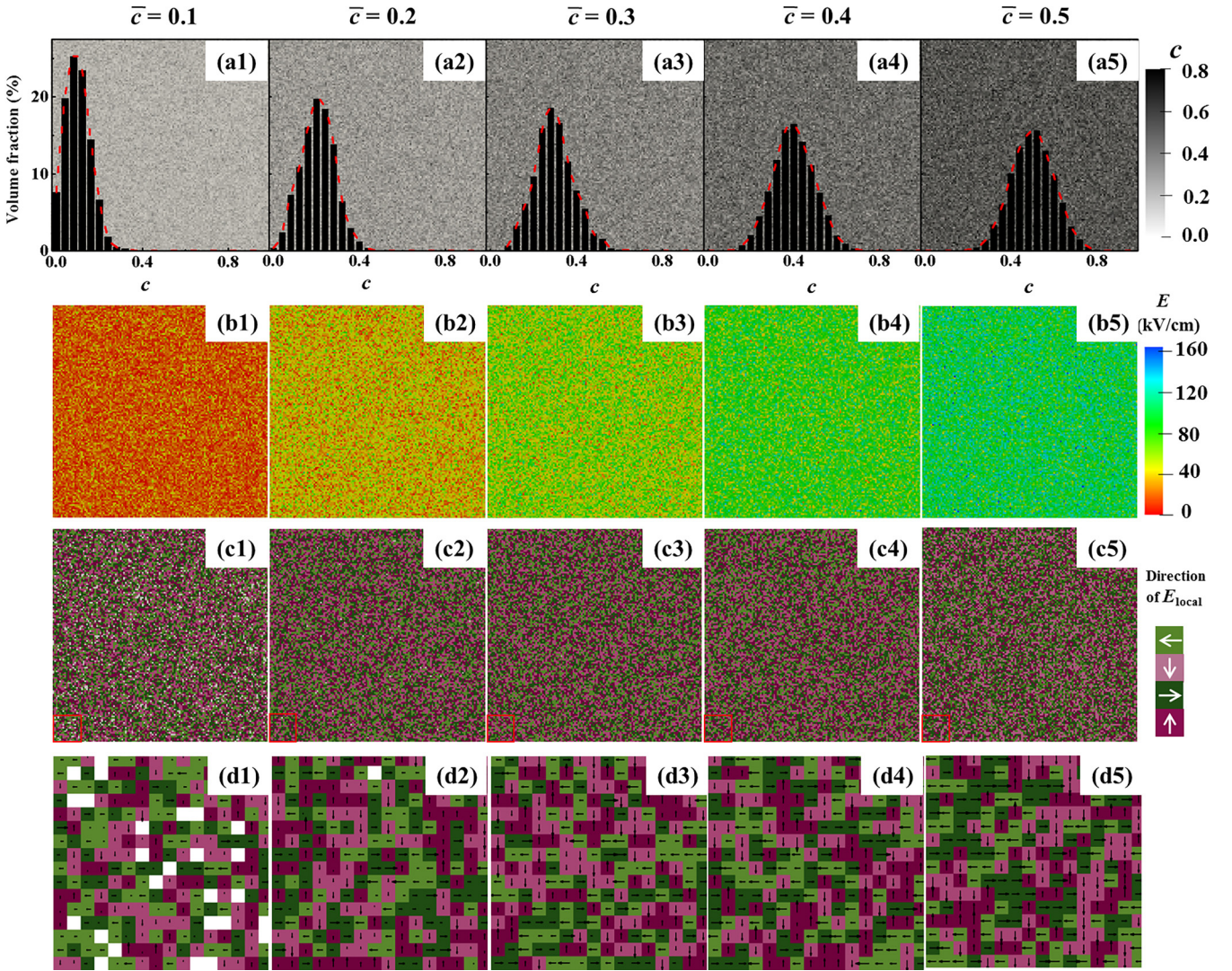
FIG. 1. Distribution of local defect concentration c (a1)–(a5), of magnitude of local electric fields $\mathbf{E}_{\text{local}}$ (b1)–(b5), of directions of local electric fields (c1)–(c5), and of local electric field vectors $\mathbf{E}_{\text{local}}$ in the small region denoted by the red square at the bottom-left corner of (c1)–(c5) and (d1)–(d5). The insets in (a1)–(a5) show the site fraction of grid points with different defect concentrations. The white pixels in (c1) and (c2) represent areas without local electric fields. The length and directions of arrows in (d1)–(d5) represent the magnitude and directions of $\mathbf{E}_{\text{local}}$, respectively.

possible diffuse interface between different regions with different defect concentrations is not considered. Figures 1(b) and 1(c) show the distribution of local electric fields in each system in terms of the magnitudes and directions, respectively. As stated above, the magnitudes of the local electric fields scale with c, and their directions are randomly distributed along the four $\langle 10 \rangle$ directions. Figure 1(d) gives the distribution of local electric fields at a small region in the system denoted by the red square at the bottom-left corner of (c1)–(c5).

In the phase-field simulations, the domain structure of a ferroelectric system is described by the spatial distribution of polarization $\mathbf{P}$ (P_1, P_2, P_3) [34,35]. The total free energy of the system F_{total} is composed of bulk chemical free energy, gradient energy, the electrostatic energy, and the elastic energy, i.e., $F = \int_V (f_{\text{bulk}} + f_{\text{gradient}} + f_{\text{electr}} + f_{\text{elastic}}) dV$, where V is the volume of the system, f_{bulk}, f_{gradient}, f_{electr}, f_{elastic} are the bulk chemical free energy density, the gradient energy density, the electrostatic energy density, and the elastic energy density, respectively. f_{bulk} is described by a sixth-order Landau polynomial:

$$
\begin{aligned}
f_{\text{bulk}} =\ & \alpha\left(P_1^2 + P_2^2 + P_3^2\right) + \beta_1\left(P_1^2 + P_2^2 + P_3^2\right)^2 \\
& + \gamma_1\left(P_1^2 + P_2^2 + P_3^2\right)^3 + \beta_2\left(P_1^2 P_2^2 + P_2^2 P_3^2 + P_1^2 P_3^2\right) \\
& + \gamma_2\left[P_1^4\left(P_2^2 + P_3^2\right) + P_2^4\left(P_1^2 + P_3^2\right) + P_3^4\left(P_1^2 + P_2^2\right)\right] \\
& + \gamma_3 P_1^2 P_2^2 P_3^2,
\end{aligned}
\tag{1}
$$

where P is the magnitude of the polarization vector $\mathbf{P}$, and α, β_1, β_2, γ_1, γ_2, γ_3 are the Landau coefficients. f_{gradient} is written as $f_{\text{gradient}} = \frac{1}{2} G_{11}[\sum_{i=1,2,3; j=1,2,3} (P_{i,j})^2]$, where G_{11} is the gradient energy coefficient. f_{electr} is calculated by $f_{\text{electr}} = -\frac{1}{2} E_i P_i - E_{\text{dep},i} P_i - E_{\text{local},i} P_i - E_{\text{ex},i} P_i$, where E_i denotes the inhomogeneous electric field due to the dipole-dipole interactions, $E_{\text{dep},i}$ is the depolarization electric field,

$E_{ex,i}$ is the external electric field, $E_{local,i}$ is the local electric field. $f_{elastic}$ is calculated by $f_{elastic} = \frac{1}{2}C_{ijkl}e_{ij}e_{kl} = \frac{1}{2}C_{ijkl}(\varepsilon_{ij} - \varepsilon_{ij}^0)(\varepsilon_{kl} - \varepsilon_{kl}^0)$, where C_{ijkl} is the elastic constants, and e_{ij}, ε_{ij}, and ε_{ij}^0 are the elastic strain, total strain, and spontaneous strain, respectively. The spontaneous strain ε_{ij}^0 is related to the polarization $\boldsymbol{P}$ by $\varepsilon_{ij}^0 = Q_{ijkl}P_kP_l$, where Q_{ijkl} is the electrostrictive coefficient. The electrostrictive coefficients and elastic constants are assumed to be compositionally independent according to experimental results [36,37]. The temporal evolution of the polarization field is obtained by solving the time-dependent Landau-Ginzburg equation:

$$\frac{\partial P_i(x,t)}{\partial t} = -M\frac{\delta F_{total}}{\delta P_i(x,t)}, \quad i = 1, 2, 3, \qquad (2)$$

where M is the kinetic coefficient and t is the time.

For computational efficiency, we first carry out our simulations in pseudo-two-dimensions (2D) with a cell size of $512 \times 512 \times 1$ grid points. The polarization along the x_3 direction is set to be zero at all grid points. Periodic boundary conditions are applied along all dimensions. The Landau coefficients of the simulated system are modified from those of BaTiO$_3$ [21,38]: $\alpha = 3.5 \times 10^5(T/°C - 120 + bc)\,C^{-2}\,m^2\,N$, $\beta_1 = -3.697 \times 10^8\,C^{-4}\,m^6N$, $\beta_2 = 1.625 \times 10^8\,C^{-4}\,m^6N$, $\gamma_1 = 8.294 \times 10^9\,C^{-6}\,m^{10}\,N$, $\gamma_2 = 4.47 \times 10^{10}\,C^{-6}\,m^{10}\,N$, $\gamma_3 = 6.91 \times 10^{10}\,C^{-6}\,m^{10}\,N$. In the current work, it is assumed that adding 10% point defects would reduce the Curie temperature by $\sim$30 °C and thus b is set to be 300. Such a value of b is in a reasonable range according to experimental results on different doped ferroelectric systems [30–32]. It is assumed that temperature is uniform in the sample, and the temperature effect on the domain structure and thus the properties of the doped ferroelectric system are characterized solely by the Landau coefficient α. Since the relaxors considered in the current study are away from the interferroelectric phase boundary and the energy barriers among different ferroelectric phases are high, all the other possible temperature effects, such as thermal stress, thermal fluctuation, and thermal transport, can be safely neglected. The electrostrictive coefficients and elastic constants adopt those of BaTiO$_3$ [39]: $C_{11} = 1.78 \times 10^{11}\,m^{-2}\,N$, $C_{12} = 9.64 \times 10^{10}\,m^{-2}\,N$, $C_{44} = 1.22 \times 10^{11}\,m^{-2}\,N$, $Q_{11} = 0.1\,C^{-1}\,m^2$, $Q_{12} = -0.034\,C^{-1}\,m^2$, and $Q_{44} = 0.029\,C^{-1}\,m^2$ (all in voigot notation). The 90° domain wall energy is assumed to be 0.01 J/m^2 [40], which yields a length scale of 5 nm.

The heat capacity (c_p) of each sample is calculated by $c_p = -T(\frac{\partial^2 F}{\partial T^2})$. The polarization ($P$) -electric field ($E$) and strain ($S$) -$E$ loops are obtained by measuring the polarization and strain of the sample during the process of applying and removing external electric fields. The zero-field-cooling (ZFC) curves of each composition are calculated by measuring the polarization of the sample during the field heating process, which follows the zero-field-cooling process. The field-cooling (FC) curves are calculated by measuring the polarization during the field heating process, which follows the field cooling process. The external electric field applied during the field heating/field cooling process is a small field with magnitude $\sim$6.5 kV/cm. The dielectric permittivity is
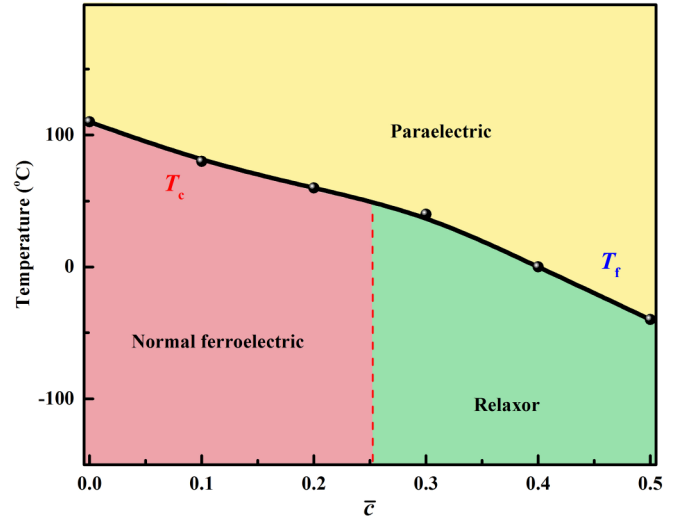

FIG. 2. Phase diagram of the doped ferroelectric system studied in this work.

calculated by recording the polarization change of the system under a small ac external electric field during multiple cycles.

III. RESULTS

A. Phase diagram of the doped ferroelectric systems

Figure 2 shows the phase diagram of the doped ferroelectric system studied in this work. In the phase diagram, the paraelectric-ferroelectric transition temperature (T_C) is determined by the peak temperature on the heat capacity (c_p) -temperature (T) curve [41], and the freezing temperature (T_f) is determined by the peak temperature on the ZFC curve [41]. The freezing temperature denotes the temperature at which the nanodomains in relaxors become frozen [42]. Note that the normal ferroelectrics and relaxor ferroelectrics are distinguished by the obvious peak at c_p-T curves of normal ferroelectrics indicating sharp ferroelectric transitions and no obvious peaks of relaxor ferroelectrics suggesting sluggish transitions. It is illustrated in Fig. 2 that at $\bar{c} <$ 0.3, normal ferroelectric transition occurs, while at $\bar{c} \geqslant 0.3$, relaxor ferroelectric transition occurs, which is consistent with their characteristics of domain structure evolution [41]. Also, the frequency dispersion of dielectric permittivity has also been obtained by the current phase-field model [41]. The simulated phase diagram given in Fig. 2 is consistent with the experimental phase diagram for a number of relaxor systems, such as Pb$_{(1-x)}$La$_x$(Zr$_{0.4}$Ti$_{0.6}$)$_{(1-x/4)}$O$_3$ [32] and BaZr$_x$Ti$_{1-x}$O$_3$ systems [43], consisting of a paraelectric field, a normal ferroelectric field, and a relaxor field.

B. Polarization-electric field (P-E) loops and strain-electric field (S-E) loops of relaxor ferroelectrics at different temperatures

The simulated P-E and S-E loops of $\bar{c} = 0.5$ relaxor at different temperatures are given in Fig. 3(a1) and 3(b1) [41]. It is seen that at all three temperatures, the P-E loops are pinched and the S-E loops are recoverable, which are qualitatively different from those predicted in previous work [21,23]. Also note that here the pinched P-E loops are obtained under
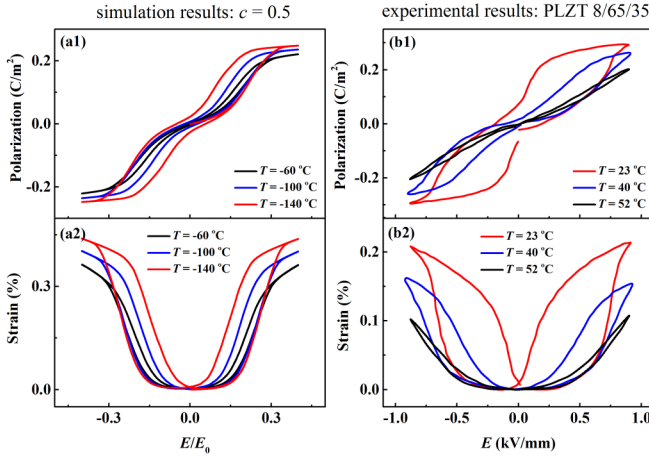
FIG. 3. (a1), (b1) The simulated *P-E* loops and *S-E* loops for $\bar{c} = 0.5$ relaxor at different temperatures. (a2), (b2) The experimental measured *P-E* loops and *S-E* loops for PLZT 8/65/35 at different temperatures [44].

FIG. 5. The domain structure evolution upon applying and removing external electric field for both normal ferroelectric ($\bar{c} = 0.1$, $T = 20\,°C$) and relaxor ferroelectric ($\bar{c} = 0.5$, $T = -140\,°C$). The external electric field is along the [10] direction.

no mechanical loading. Although the phase-field simulation work performed by Yang *et al.* also predicts a similar pinched *P-E* loop, it was obtained under mechanical loading [22]. With decreasing temperature, the polarization and electrostrain increase and so does the hysteresis [41]. Figures 3(a2) and 3(b2) plot the experimentally measured *P-E* and *S-E* loops of $(Pb_{0.92}La_{0.08})(Zr_{0.65}Ti_{0.35})_{0.98}O_3$ (PLZT 8/65/35) at three different temperatures [44], which clearly demonstrates that the simulated *P-E* loops and *S-E* loops qualitatively agree with the experimentally measured ones. Similar experimental results have been reported in a number of other doped ferroelectric systems such as $[(1)–x]BaTiO_{3–x}Bi(Zn_{1/2}Ti_{1/2})O_3$ [45] and $[(1)–x](Bi_{0.5}Na_{0.5})TiO_{3–x}SrTiO_3$ [46].

Note that the pinched *P-E* loops and recoverable *S-E* loops shown above in Fig. 3 are qualitatively different from the "slim" *P-E* and *S-E* loops of relaxor ferroelectrics obtained in Ref. [21]. First, the slim *P-E* loop is not pinched. To better illustrate this, Fig. 4 shows the variation of the slopes of *P-E*
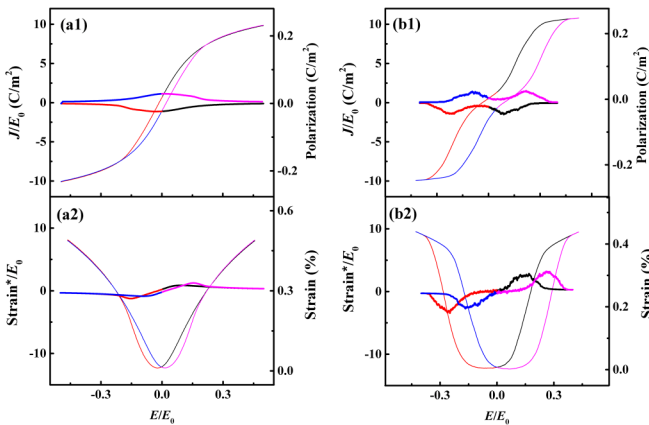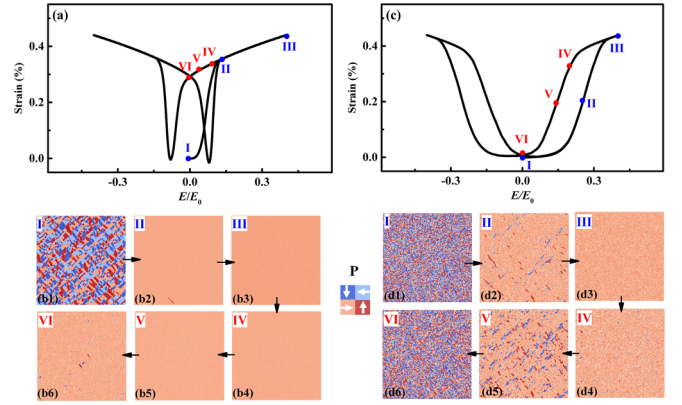

FIG. 4. (a1), (a2) The slope of *P-E* and *S-E* loops for the slim *P-E* and *S-E* loops. *J* is the slope of the *P-E* loop and strain* is the slope of the *S-E* loop. (b1), (b2) The slope of *P-E* and *S-E* loops for the pinched *P-E* loops and recoverable *S-E* loops.

and *S-E* loops with external electric fields for a slim *P-E* loop and an *S-E* loop obtained in Ref. [21] as well as for a pinched *P-E* loop and a recoverable *S-E* loop given above [41]. It is demonstrated that for the pinched *P-E* loop, the slope approaches zero at zero external electric field, while for the slim *P-E* loop it becomes maximum. Second, the origins of the small remnant polarization and the small remnant strain for the two cases are different. For the slim *P-E* and *S-E* loops of relaxors obtained in Ref. [21], the system is more in the hysteresis-free paraelectric state with a small portion of embedded hysteretic ferroelectric domains, and the recoverability of polarization and strain is mostly caused by the paraelectric phase [41]. On the other hand, for the pinched *P-E* loop and the recoverable electrostrain obtained in this work, the system is in a ferroelectric nanodomain state with a negligible portion of paraelectric phase, and the recoverability of polarization and strain is caused by the recoverable ferroelectric nanodomains, which will be discussed in detail below.

IV. DISCUSSIONS

A. Origin of pinched hysteresis loops and recoverable electrostrains in relaxor ferroelectrics

To investigate the origin of the recoverability of polarization and electrostrain of relaxor compositions as shown in Fig. 4, the evolutions of domain structure upon application and removal of an external electric field for both normal ferroelectrics ($\bar{c} = 0.1$, $T = 20\,°C$) and relaxor ferroelectrics ($\bar{c} = 0.5$, $T = -140\,°C$) are shown in Fig. 5, together with their strain-electric-field loops. It indicates that for normal ferroelectrics ($\bar{c} = 0.1$, $T = 20\,°C$), the external electric field transforms from the initial multidomain state [Fig. 5(b1)] to the single-domain state [Fig. 5(b3)] under an applied electric field. Upon removal of the electric field, the single-domain state is largely maintained, except at some local regions new domains appear [Fig. 5(b6)]. On the other hand, for relaxor ferroelectrics ($\bar{c} = 0.5$, $T = -140\,°C$), with the application of an electric field, the nanodomains with the polarization direction in the field direction gradually grow at the expense of nanodomains with their polarization direction not in the field
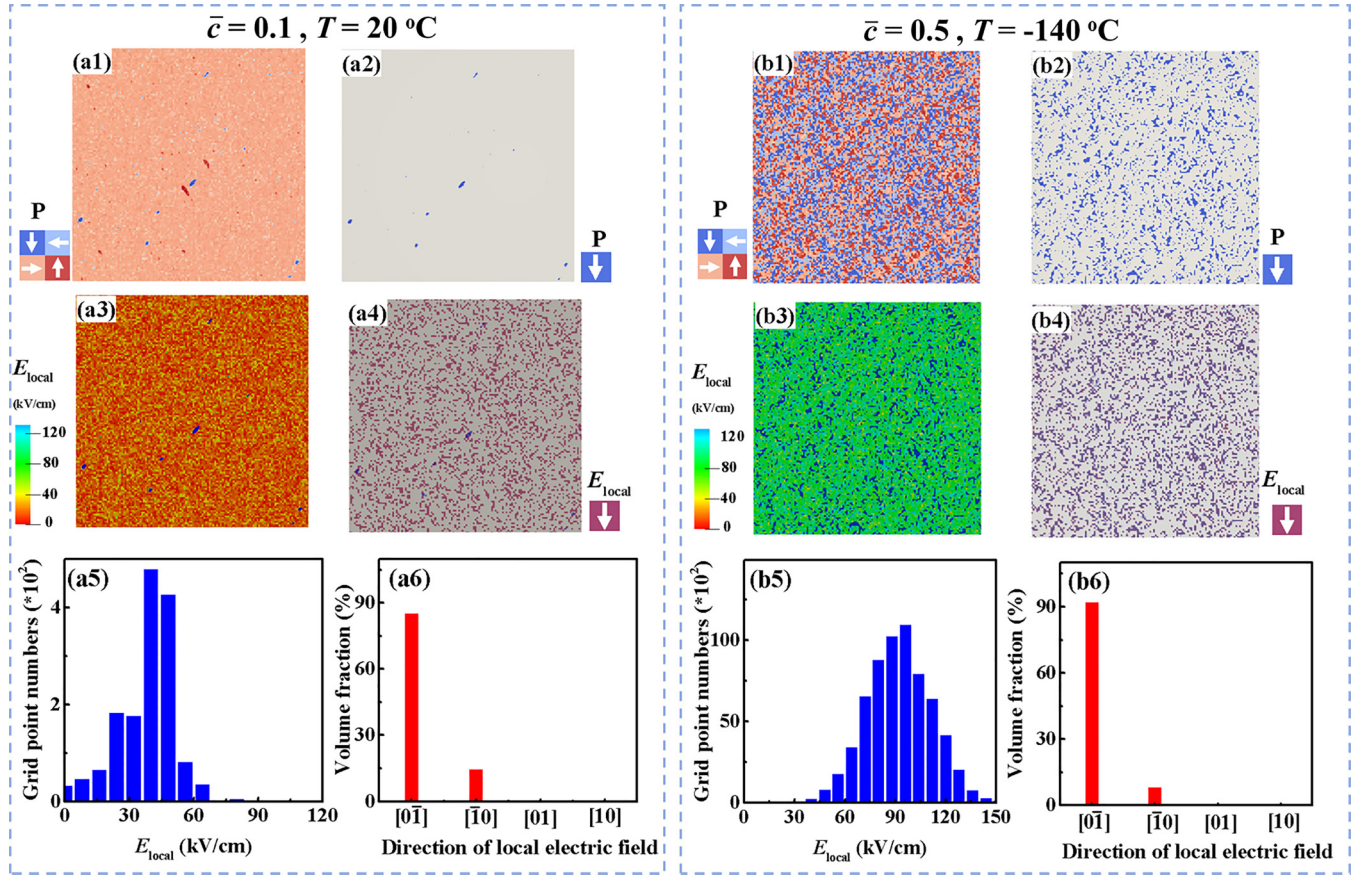
FIG. 6. The relationship between the recoverability of electrostrain and the magnitudes/directions of local electric fields. (a1), (b1) The domain structure at point VI in the electrostrains shown in Fig. 5 for normal ferroelectric ($\bar{c} = 0.1$, $T = 20\,°C$) and relaxor ($\bar{c} = 0.5$, $T = -140\,°C$). (a2), (b2) The distribution of domains with polarization directions along [0$\bar{1}$] (which is called "these new domains" below) extracted from (a1) and (b1). (a3), (b3) The positions where local electric fields are along the [0$\bar{1}$] direction as well as the positions of these new domains. (a4), (b4) The magnitude of local electric fields at these new domains. (a5), (b5) The number of grid points with different magnitudes of local electric fields at these new domains. (a6), (b6) The volume fraction of grid points with different directions of local electric fields at these new domains.

direction, and, at a large enough field, a nearly single-domain state [Fig. 5(d3)] is induced. Upon removing the electric field, new domains with other directions gradually nucleate and grow, and at zero field the initial multidomain state almost recovers completely [Fig. 5(d6)].

To understand why the initial domain structures and thus the polarizations and electrostrains could recover for the relaxor ferroelectrics but not for the normal ferroelectrics as shown in Fig. 5, more analysis is performed. Figures 6(a2) and 6(b2) plot the positions of domains with their polarizations along the [0$\bar{1}$] direction (which will be referred to as "*these new domains*" hereinafter; note that other new domains with polarizations along the [10] and [$\bar{1}$0] directions should demonstrate a similar tendency), which are extracted from the domain structures at point VI in Fig. 5 for normal ferroelectric ($\bar{c} = 0.1$, $T = 20\,°C$) and relaxor ($\bar{c} = 0.5$, $T = -140\,°C$) [which is given in Figs. 6(a1) and 6(b1)], respectively. Figures 6(a3) and 6(b3) show the position where the local electric fields are along the [0$\bar{1}$] direction as well as the positions of these new domains. It is illustrated that most of these new domains are with local electric fields along the [0$\bar{1}$] direction, which is further evidenced by the site fraction of the grid points with different directions from the local electric fields

for these new domains given in Figs. 6(a6) and 6(b6). On the other hand, Figs. 6(a4) and 6(b4) display the magnitudes of the local electric fields at these new domains. To better illustrate the tendency, Figs. 6(a5) and 6(b5) plot the number of grid points with different magnitudes of the local electric fields at these new domains. They indicate that most of these new domains are at the positions with relatively large local electric fields (>30 kV/cm). Thus, it can be concluded that large local electric fields along the direction of spontaneous polarizations can assist in the nucleation of new domains and thus help recover the initial polarization and strain. For relaxors, as the local electric fields at most positions are large (>30 kV/cm), nucleation of domains along the local field direction becomes easy and thus the initial domain structure and polarization/strain could be recovered. On the other hand, nucleation of new domains could only occur at limited local regions for normal ferroelectrics because the local electric fields are not large enough at most positions.

B. Effects of the directions of local electric fields on the recoverability of polarization and electrostrain

To further demonstrate that the local electric fields along the directions of spontaneous polarizations assist in the
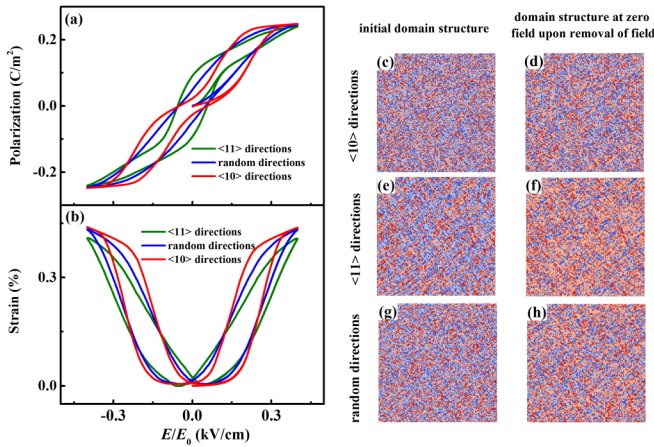
FIG. 7. Effect of directions of local electric fields on the recoverability of polarizations and electrostrains for relaxor ferroelectric ($\bar{c} = 0.5$, $T = -140\,^{\circ}$C). (a) Polarization hysteresis loops of the three systems with different directions of local electric fields. (b) Electrostrains of the three systems. (c)–(h) Initial domain structure and the domain structure at zero external field upon removal of external electric field for the three systems.

nucleation of new domains and thus the recovery of polarizations and electrostrains, two control systems, A and B, are studied in which the magnitude of local electric fields is kept the same as that of the studied system, but the directions are different. In system A, the directions of the local electric fields are along the $\langle 11 \rangle$ directions. In system B, the directions of the local electric field are in all directions. Figures 7(a) and 7(b) give the polarization hysteresis loops and electrostrains of these two control systems along with those of the system studied above, in which the directions of the local electric fields are along the $\langle 10 \rangle$ directions. The results show that for both control systems, the recoverability of polarization and electrostrain becomes less obvious than that for the system studied above [41]. Figures 7(c)–7(h) give the initial domain structures before applying the external electric fields and the domain structures at zero electric field upon removal of external fields for the three systems, which clearly indicate that the domain structure does not recover to itself for the two control systems (systems A and B). This is because the directions of the spontaneous polarization in the doped ferroelectric system (T ferroelectric phase) are along the $\langle 10 \rangle$ directions. Under local electric fields with [01], [10], [0$\bar{1}$], and [$\bar{1}$0] directions, the new T domains are easier to nucleate. Therefore, when the local electric fields are in the same directions as those of the spontaneous polarizations, recoverable electrostrain could be easily obtained.

C. Implications for designing relaxor ferroelectrics with large recoverable electrostrain

Note that the studied doped ferroelectric system is a model system, thus the analysis and conclusions present in this work should be applicable qualitatively to a group of relaxors that are away from the interferroelectric phase boundary. To further demonstrate this, another two cases with different Landau parameters are simulated. One is changing the parameter b

to be 700, and the other is using an eighth-order Landau polynomial rather than a sixth-order one [Eq. (1)]. Pinched P-E loops and recoverable S-E loops are obtained in both cases as long as the directions of local electric fields caused by defect dipoles are set to be along the spontaneous polarization directions [41].

The above simulation results indicate that the recoverability of electrostrain of relaxor ferroelectrics originates from the large local electric fields along the spontaneous polarization directions, which can facilitate the nucleation of new polarization domains as the external electric field is decreasing. Such results could explain why a pinched hysteresis loop and recoverable electrostrain are frequently reported in heterovalent-doping-induced relaxors [7–11], but not found in isovalent-doping-induced relaxor systems such as $BaZr_{0.3}Ti_{0.7}O_3$ [13] and $Ba_{1-x}Sr_xSn_yTi_{1-y}O_3$ relaxors [14]. This is because, in heterovalent-doping ferroelectric systems, the magnitudes of the local electric fields are stronger than those in isovalent-doping ferroelectric systems because of the charge mismatch in the former. In addition, it could help to explain why pinched polarization hysteresis loops and thus recoverable electrostrains are experimentally found in $La_xPb_{1-x}(Zr_{0.65}Ti_{0.35})_{1-x/4}O_3$ relaxors [11,44,47], but not observed in $La_xPb_{1-x}(Zr_{0.4}Ti_{0.6})_{1-x/4}O_3$ relaxors [48], although both systems are heterovalent-doping relaxor systems. This is because, in $PbZr_{0.4}Ti_{0.6}O_3$ ferroelectric, the directions of spontaneous polarization (T phase) are along the $\langle 100 \rangle$ directions, while in $PbZr_{0.65}Ti_{0.35}O_3$ ferroelectrics, the directions of spontaneous polarization (R phase) are along the $\langle 111 \rangle$ directions [49]. On the other hand, the directions of local electric fields caused by La doping in a $La_xPb_{1-x}(Zr_yTi_{1-y})_{1-x/4}O_3$ system are close to the $\langle 111 \rangle$ directions [24,50], thus recoverable electrostrain is easier to achieve in $La_xPb_{1-x}(Zr_{0.65}Ti_{0.35})_{1-x/4}O_3$ relaxors.

Therefore, to achieve large recoverable electrostrain, it is essential to carefully choose the type of point defects doped into ferroelectric systems. It is better that the point defects can lead to strong local electric fields aligned in the directions of spontaneous polarizations in the ferroelectric system, i.e., the defect dipole should be along the bulk spontaneous polarization directions [50]. This work thus demonstrates that defect dipole engineering could be an effective way to obtain large recoverable electrostrain in relaxors.

D. 3D simulation results

The above results are obtained in 2D simulations. Figure 8 shows the result from a 3D simulation of a relaxor sample ($\bar{c} = 0.5$, $T = -140\,^{\circ}$C) where the directions of local electric fields caused by point defects are along the six spontaneous polarization directions of the tetragonal ferroelectric phase (i.e., [100], [010], [001], [$\bar{1}$00], [0$\bar{1}$0], and [00$\bar{1}$]). The pinched polarization hysteresis loop and recoverable electrostrain are clearly demonstrated [Fig. 8(a)]. Figures 8(b1) and 8(b2) show the domain structures of the relaxor before applying an external electric field and after removing the external fields, respectively. It is readily seen that the domain structure could almost fully recover to the initial state because of the strong local electric fields in spontaneous polarization directions.
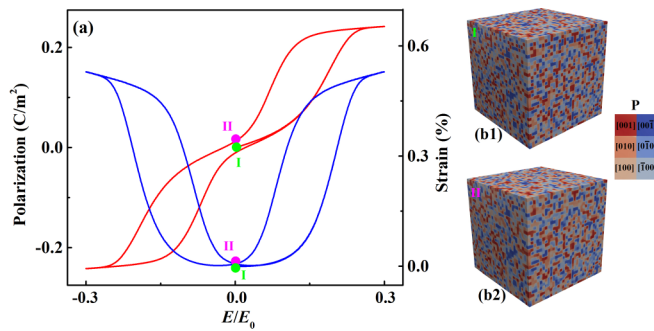
FIG. 8. (a) *P-E* loop and *S-E* loop of a relaxor sample in 3D ($\bar{c} = 0.5$, $T = -140\,^\circ$C). (b1) Initial domain structure before applying external electric fields. (b2) The domain structure at zero field after removing external fields.

Thus, the results and conclusions obtained in 2D and 3D simulations are consistent.

V. CONCLUSIONS

We have systematically investigated the polarization hysteresis loops and electrostrains of both normal ferroelectrics and relaxor ferroelectrics of doped ferroelectric systems by using phase-field simulations. In the phase-field model, we consider both local electric fields and local phase-transition temperature variations induced by the local compositional heterogeneity. Different from previous models in which the directions of local electric fields are randomly distributed along all directions, the directions of the local electric fields are randomly distributed *only along the spontaneous polarization directions of the system*. We found that the normal ferroelectrics exhibit a single polarization hysteresis loop and butterfly-shaped electrostrain, while the relaxor ferroelectrics exhibit a pinched hysteresis loop and recoverable electrostrain, which is consistent with reports in some doped ferroelectric systems. The recoverability of polarization and electrostrain in the relaxor ferroelectrics has been ascribed to the large local electric fields caused by point defects, which could assist in nucleation of new domains with polarization directions along the spontaneous polarization directions and thus could help recover the initial multidomain state, polarization, and electrostrain. We also found that if the directions of the local electric fields are not along the spontaneous polarization directions, the recoverability of electrostrain would be greatly inhibited. This work unravels the origin of large recoverable electrostrains found in many relaxor ferroelectrics. It could guide the design of relaxor ferroelectric materials with large recoverable electrostrains.

[1] Kenji Uchino, *Ferroelectric Devices* (CRC, Boca Raton, FL, 2018).

[2] G. H. Haertling, Ferroelectric ceramics: History and technology, J. Am. Ceram. Soc. **82**, 797 (1999).

[3] X. Ren, Large electric-field-induced strain in ferroelectric crystals by point-defect-mediated reversible domain switching, Nat. Mater. **3**, 91 (2004).

[4] W. Pan, Q. Zhang, A. S. Bhalla, and L. E. Cross, Field-induced strain in single-crystal BaTiO$_3$, J. Am. Ceram. Soc. **71**, C-302 (1988).

[5] N. Srivastava and G. J. Weng, A theory of double hysteresis for ferroelectric crystals, J. Appl. Phys. **99**, 054103 (2006).

[6] Y. Ji, Q. Li, F. Zhuo, Q. Yan, Y. Zhang, and X. Chu, Reversible and high-temperature-stabilized strain in (Pb, La)(Zr, Sn, Ti)O$_3$ antiferroelectric ceramics, ACS Appl. Mater. Interfaces **11**, 32135 (2019).

[7] S.-T. Zhang, A. B. Kounga, E. Aulbach, H. Ehrenberg, and J. Rödel, Giant strain in lead-free piezoceramics Bi$_{0.5}$Na$_{0.5}$TiO$_3$–BaTiO$_3$–K$_{0.5}$Na$_{0.5}$NbO$_3$ system, Appl. Phys. Lett. **91**, 112906 (2007).

[8] G. Dong, H. Fan, J. Shi, and M. Li, Composition- and temperature-dependent large strain in $(1-x)$ (0.8Bi$_{0.5}$Na$_{0.5}$TiO$_3$−0.2Bi$_{0.5}$K$_{0.5}$TiO$_3$)−xNaNbO$_3$ ceramics, J. Am. Ceram. Soc. **98**, 1150 (2015).

[9] J. Hao, B. Shen, J. Zhai, C. Liu, X. Li, and X. Gao, Switching of morphotropic phase boundary and large strain response in lead-free ternary (Bi$_{0.5}$Na$_{0.5}$)TiO$_3$−(K$_{0.5}$Bi$_{0.5}$)TiO$_3$−(K$_{0.5}$Na$_{0.5}$)NbO$_3$ system, J. Appl. Phys. **113**, 114106 (2013).

[10] S.-T. Zhang, A. B. Kounga, W. Jo, C. Jamin, K. Seifert, T. Granzow, J. Rödel, and D. Damjanovic, High-strain lead-free antiferroelectric electrostrictors, Adv. Mater. **21**, 4716 (2009).

[11] E. T. Keve and A. D. Annis, Studies of phases, phase transitions and properties of some PLZT ceramics, Ferroelectrics **5**, 77 (1973).

[12] W. Jo, T. Granzow, E. Aulbach, J. Rodel, and D. Damjanovic, Origin of the large strain response in (K$_{0.5}$Na$_{0.5}$)NbO$_3$-modified (Bi$_{0.5}$Na$_{0.5}$)TiO$_3$-BaTiO$_3$ lead-free piezoceramics, J. Appl. Phys. **105**, 094102(2009).

[13] Z. Yu, C. Ang, R. Guo, and A. S. Bhalla, Ferroelectric-relaxor behavior of Ba(Ti$_{0.7}$Zr$_{0.3}$)O$_3$ ceramics, J. Appl. Phys. **92**, 2655 (2002).

[14] C. Molin, T. Richter, and S. E. Gebhardt, Tailoring electrocaloric properties of Ba$_{1-x}$Sr$_x$Sn$_y$Ti$_{1-y}$O$_3$ ceramics by compositional modification, J. Eur. Ceram. Soc. **42**, 140 (2022).

[15] R. A. Cowley, S. N. Gvasaliya, S. G. Lushnikov, B. Roessli, and G. M. Rotaru, Relaxing with relaxors: A review of relaxor ferroelectrics, Adv. Phys. **60**, 229 (2011).

[16] D. Wang, X. Ke, Y. Wang, J. Gao, Y. Wang, L. Zhang, S. Yang, and X. Ren, Phase diagram of polar states in doped ferroelectric systems, Phys. Rev. B **86**, 054120 (2012).

[17] T. Li, C. Liu, X. Ke, X. Liu, L. He, P. Shi, X. Ren, Y. Wang, and X. Lou, High electrostrictive strain in lead-free relaxors near the morphotropic phase boundary, Acta Mater. **182**, 39 (2020).

[18] V. V. Shvartsman, W. Kleemann, J. Dec, Z. K. Xu, and S. G. Lu, Diffuse phase transition in $BaTi_{1-x}Sn_xO_3$ ceramics: An intermediate state between ferroelectric and relaxor behavior, J. Appl. Phys. **99**, 124111 (2006).

[19] D. Phelan, C. Stock, J. A. Rodriguez-Rivera, S. Chi, J. Leão, X. Long, Y. Xie, A. A. Bokov, Z.-G. Ye, P. Ganesh, and P. M. Gehring, Role of random electric fields in relaxors, Proc. Natl. Acad. Sci. USA **111**, 1754 (2014).

[20] G. Smolensky, Ferroelectrics with diffuse phase transition, Ferroelectrics **53**, 129 (1984).

[21] Z. Hong, X. Ke, D. Wang, S. Yang, X. Ren, and Y. Wang, Role of point defects in the formation of relaxor ferroelectrics, Acta Mater. **225**, 117558 (2022).

[22] S. Wang, M. Yi, and B.-X. Xu, A phase-field model of relaxor ferroelectrics based on random field theory, Int. J. Solids Struct. **83**, 142 (2016).

[23] S. T. Lau, J-M. Liu, H. L. W. Chan, and C. L. Choy, A Monte Carlo simulation on domain pattern and ferroelectric behaviors of relaxor ferroelectrics, J. Mater. Sci. **41**, 163 (2006).

[24] A. Chandrasekaran, D. Damjanovic, N. Setter, and N. Marzari, Defect ordering and defect–domain-wall interactions in $PbTiO_3$: A first-principles study, Phys. Rev. B **88**, 214116 (2013).

[25] R.-A. Eichel, P. Erhart, P. Träskelin, K. Albe, H. Kungl, and M. J. Hoffmann, Defect-dipole formation in copper-doped $PbTiO_3$ ferroelectrics, Phys. Rev. Lett. **100**, 095504 (2008).

[26] Z.-H. Zhao, Y. Dai, and F. Huang, The formation and effect of defect dipoles in lead-free piezoelectric ceramics: A review, Sustain. Mater. Technol. **20**, e00092 (2019).

[27] Y. Yang, Y. Ji, M. Fang, Z. Zhou, L. Zhang, and X. Ren, Morphotropic relaxor boundary in a relaxor system showing enhancement of electrostrain and dielectric permittivity, Phys. Rev. Lett. **123**, 137601 (2019).

[28] E. Buixaderas, I. Gregora, S. Kamba, J. Petzelt, and M. Kosec, Raman spectroscopy and effective dielectric function in PLZT x/40/60, J. Phys. Condens. Matter **20**, 345229 (2008).

[29] B. Vincenzo, S. Tripathi, V. Petkov, M. Dapiaggi, M. Deluca, A. Gajović, and Y. Ren, Average and local atomic-scale structure in $BaZr_xTi_{1-x}O_3$ ($x = 0.10, 0.20, 0.40$) ceramics by high-energy X-ray diffraction and Raman spectroscopy, J. Phys.: Condens. Matter **26**, 065901 (2014).

[30] S. J. Kuang, X. G. Tang, L. Y. Li, Y. P. Jiang, and Q. X. Liu, Influence of Zr dopant on the dielectric properties and Curie temperatures of $Ba(Zr_xTi_{1-x})O_3$ ($0 \leqslant x \leqslant 0.12$) ceramics, Scr. Mater. **61**, 68 (2009).

[31] V. B. Shirokov, V. I. Torgashev, A. A. Bakirov, and V. V. Lemanov, Concentration phase diagram of $Ba_xSr_{1-x}TiO_3$ solid solutions, Phys. Rev. B **73**, 104116 (2006).

[32] Z. Sun, D. Xue, H. Wu, Y. Ji, X. Ding, D. Wang, Y. Yang, and X. Ren, Time-dependent ferroelectric transition in $Pb_{(1-x)}(Zr_{0.4}Ti_{0.6})_{(1-x/4)}O_{3-x}$La system, Appl. Phys. Lett. **102**, 222907 (2013).

[33] W. Kleemann, Random fields in relaxor ferroelectrics—a jubilee review, J. Adv. Dielectr. **2**, 1241001 (2012).

[34] S. Choudhury, Y. L. Li, C. E. Krill III, and L-Q. Chen, Phase-field simulation of polarization switching and domain evolution in ferroelectric polycrystals, Acta Mater. **53**, 5313 (2005).

[35] X. Ke, D. Wang, X. Ren, and Y. Wang, Polarization spinodal at ferroelectric morphotropic phase boundary, Phys. Rev. Lett. **125**, 127602 (2020).

[36] F. Li, L. Jin, Z. Xu, and S. Zhang, Electrostrictive effect in ferroelectrics: An alternative approach to improve piezoelectricity, Appl. Phys. Rev. **1**, 011103 (2014).

[37] R. Yuan, D. Xue, Y. Zhou, X. Ding, J. Sun, and D. Xue, Ferroelectric, elastic, piezoelectric, and dielectric properties of $Ba(Ti_{0.7}Zr_{0.3})O_{3-x}(Ba_{0.82}Ca_{0.18})TiO_3$ Pb-free ceramics, J. Appl. Phys. **122**, 044105 (2017).

[38] Y. L. Li, L. E. Cross, and L. Q. Chen, A phenomenological thermodynamic potential for $BaTiO_3$ single crystals, J. Appl. Phys. **98**, 064101 (2005).

[39] J. J. Wang, F. Y. Meng, X. Q. Ma, M. X. Xu, and L. Q. Chen, Lattice, elastic, polarization, and electrostrictive properties of $BaTiO_3$ from first-principles, J. Appl. Phys. **108**, 034107 (2010).

[40] J. Hlinka and P. Marton, Phenomenological model of a 90 domain wall in $BaTiO_3$-type ferroelectrics, Phys. Rev. B **74**, 104104 (2006).

[41] See Supplemental Material at http://link.aps.org/supplemental/10.1103/PhysRevB.109.035150 for c_p-T curves of studied compositions; the ZFC/FC curves of relaxor compositions; the evolution of domain structure with temperature of all compositions; the dielectric permittivity-temperature spectrum at different frequencies for $c = 0.5$ relaxor; the P-E and S-E loops of all compositions at different temperatures; variation of maximum polarization, maximum strain, and polarization/strain hysteresis with temperature for the simulated $c = 0.5$ relaxor and experimental PLZT 8/65/35 sample; variation of the slopes of P-E and S-E loops with external electric fields for a rectangular-like polarization hysteresis loop and a butterfly-shaped electrostrain loop of a normal ferroelectric; the domain structure evolution during application and removal of external electric field for a slim P-E and S-E loop; the difference between the remnant strain and the initial strain for the two control systems and the system studied in this work; and pinched P-E loops and corresponding recoverable S-E loops obtained in another two cases.

[42] X. Ren, Strain glass and ferroic glass–Unusual properties from glassy nano-domains, Phys. Status Solidi B **251**, 1982 (2014).

[43] T. Maiti, R. Guo, and A. S. Bhalla, Structure-property phase diagram of $BaZr_xTi_{1-x}O_3$ system, J. Am. Ceram. Soc. **91**, 1769 (2008).

[44] L. X. Zhang, X. Ren, Y. Wang, X. Q. Ke, X. D. Ding, and J. Sun, Novel electro-strain-effect in La-doped Pb(Zr,Ti)O₃ relaxor ferroelectrics, *18th IEEE International Symposium on the Applications of Ferroelectrics* (IEEE, Piscataway, NJ, 2009), pp. 1–4.

[45] N. Triamnak, R. Yimnirun, J. Pokorny, and D. P. Cann, Relaxor characteristics of the phase transformation in $(1-x)BaTiO_{3-x}Bi(Zn_{1/2}Ti_{1/2})O_3$ perovskite ceramics, J. Am. Ceram. Soc. **96**, 3176 (2013).

[46] Y. Hiruma, Y. Imai, Y. Watanabe, H. Nagata, and T. Takenaka, Large electrostrain near the phase transition temperature of $(Bi_{0.5}Na_{0.5})TiO_3$–$SrTiO_3$ ferroelectric ceramics, Appl. Phys. Lett. **92**, 262904 (2008).

[47] G. H. Haertling, Improved hot-pressed electrooptic ceramics in the (Pb,La)(Zr,Ti)O$_3$ system, J. Am. Ceram. Soc. **54**, 303 (1971).

[48] X. Dai, Z. Xu, and D. Viehland, Normal to relaxor ferroelectric transformations in lanthanum-modified tetragonal-structured lead zirconate titanate ceramics, J. Appl. Phys. **79**, 1021 (1996).

[49] D. E. Cox, B. Noheda, G. Shirane, Y. Uesu, K. Fujishiro, and Y. Yamada, Universal phase diagram for high-piezoelectric perovskite systems, Appl. Phys. Lett. **79**, 400 (2001).

[50] L. Lai,, B. Li, S. Tian, Z. Zhao, S. Zhang, and Y. Dai, Giant electrostrain in lead-free textured piezoceramics by defect dipole design, Adv. Mater. **35**, 2300519 (2023).